


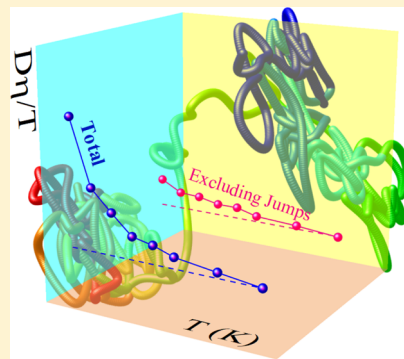
Decoupling of Translational Diffusion from the Viscosity of Supercooled Water: Role of Translational Jump Diffusion

Shivam Dueby,[†] Vikas Dubey,[†] and Snehasis Daschakraborty^{*†}

Department of Chemistry, Indian Institute of Technology Patna, Bihar 801106, India

 Supporting Information

ABSTRACT: Some experiments have witnessed gradual decoupling of viscosity from the translational self-diffusion of supercooled water with decreasing temperature. This indicates the breakdown of the Stokes–Einstein equation in supercooled water. While some theoretical and computer simulation studies indicated the jump translation of the molecules as a probable origin of the above decoupling, direct quantitative evidence is still lacking. Through a molecular dynamics (MD) simulation study, along with careful consideration of translational jump motion, we have found the most definite proof of increasing relevance of translational jump diffusion in the above decoupling phenomena. By separating the jump-only diffusion contribution from the overall diffusion of the water, we obtain the residual diffusion coefficient, which remains strongly coupled to the viscosity of the medium at the supercooled regime. These new findings can help to elucidate many experimental studies featuring molecular transport properties, where strong diffusion–viscosity decoupling is present.



1. INTRODUCTION

There are intriguing properties of supercooled water, including a strong decoupling between its viscosity and the diffusion of the molecules. Some experimental studies^{1–3}—including that by Dehaoui et al.⁴—have directly or indirectly revealed an increasing decoupling of viscosity η from the translational diffusion coefficient D of water upon cooling. This indicates a breakdown of the Stokes–Einstein (SE) relation ($D \propto T/\eta$) as the temperature decreases below $2.1 T_g$, where T_g is the glass-transition temperature. In contrast, the rotational diffusion D_r remains coupled with η for a wider range of temperature, which implies the validity of the Stokes–Einstein–Debye relation at a broader range of temperature.⁴ Similar decoupling between D and η was also reported earlier in other molecular glass-forming liquid.^{5–13} The SE equation is obeyed at a sufficiently high temperature but severely breaks down below $T \approx 1.3 T_g$. On the contrary, the rotational diffusion of the molecular glass-forming liquid and the medium viscosity remain hydrodynamically coupled with each other even at the temperature very close to T_g .^{7,8,14}

Deeply supercooled liquids have spatially heterogeneous dynamics, which have been confirmed by various experiments^{5,6,15–18} and computer simulation studies.^{19–23} Some computer simulation studies have indicated that the emerging spatiotemporal heterogeneities in supercooled water and other supercooled liquids have a strong connection with the increasing violation of the SE relation with decreasing temperature.^{24–31} The violation of the SE relation in supercooled water is also explained by the crossing of the Widom line, arising from the liquid–liquid critical point (LLCP).³² In this context, it is important to mention the

Goldstein's hypothesis on the effect of temperature on the mechanism of translation of liquid molecules.³³ The theory states that the liquid molecules translate in the rugged free-energy landscape via hopping from one free energy well to another via crossing the saddle points at low temperature. However, the same molecules diffuse freely by the Brownian motion at a higher temperature when the thermal energy becomes comparable to or higher than the heights of the barriers of the rugged free-energy landscape. This hypothesis was supported by many theoretical and computer simulation studies,^{34–40} which indicated the presence of translational jump of molecules and its connection with the breakdown of the SE relation in the supercooled liquid. Recent works have shown that the rotation-assisted translational movement of solvent water around a solute induces translational jump diffusion of a tracer from one solvent cage to another in supercooled water.²⁴

Even though the prior studies have implied the pivotal role of the translational jump of molecules for the breakdown of the SE relation in supercooled water, a more direct quantitative connection in between the two is still lacking. This work is an attempt of MD simulation to establish a direct connection between the jump diffusion D_{jump} and the violation of the SE relation. Here, we directly evaluate D_{jump} of the water molecules and subsequently separate the same from the total diffusion D of the water molecules. The above decomposition allows us to check the coupling of the viscosity with different

Received: February 22, 2019

Revised: July 22, 2019

Published: July 30, 2019

components of D and thereby gain further insights into the role of the translational jump diffusion of the water molecules for the increasing breakdown of the SE relation with decreasing temperature.

The organization for the remainder of this paper is as follows. The method and model, including the simulation details, are detailed in Section 2. Section 3 details the simulation results and discussions. Concluding remarks are offered in Section 4.

2. METHOD AND MODEL

2.1. Simulation Details. We have used the GROMACS package⁴¹ for performing the MD simulations. We have considered 2000 water molecules, which are placed in a cubic simulation box with periodic boundary conditions employed in all sides. The water molecules are modeled by the TIP4P/2005 force field,⁴² which is one of the most successful water models in predicting various thermodynamic, structural, and dynamical properties at a wide range of temperatures including the deeply supercooled regime.

We have simulated eight different temperatures: 210, 220, 230, 240, 250, 260, 280, and 300 K at 1 bar pressure. The first five temperatures represent the supercooled state of water because TIP4P/2005 water freezes at 252 K.⁴² Each of these systems is equilibrated for 50 ns time, during which the temperature is kept constant at the respective desired temperatures using the Nosé–Hoover thermostat^{43,44} and the pressure at 1 bar using the Parrinello–Rahman barostat.⁴⁵ We have chosen 0.5 ps times for both the pressure and temperature coupling constant. We extend each of the simulations for a sufficiently long time for obtaining the production trajectory for analyses, which aggregates to a total of 2.5 μ s simulation time. The production trajectory durations t_{traj} for the simulations at different temperatures are detailed in Table 1.

Table 1. Production Trajectory Duration t_{traj} for Simulations at Different Temperatures

T (K)	production trajectory length t_{traj} (ns)
210	500
220	500
230	400
240	400
250	300
260	200
280	100
300	100

We have used the Leapfrog–Verlet algorithm for solving the equations of motions every 2 fs time. The production trajectory is saved at a regular interval of 100 fs for $T < 280$ K and 20 fs otherwise. The higher time resolution of the trajectories at a higher temperature is required for correct estimation of the viscosity coefficient. A cutoff distance around half of the box length is applied for Lennard–Jones interactions. Particle mesh Ewald summation technique and LINCS algorithm⁴⁶ are used to handle the long-range Coulomb interactions and to constrain the water O–H bonds, respectively.

The validity of the above simulation protocol is ensured by good agreement of various simulated quantities (such as densities, diffusion, viscosity, and so forth) with earlier

experimental and simulated dynamical quantities. Figure S1 (Section S1) of the Supporting Information presents the comparison between the present simulated densities with earlier experimental^{47–49} and simulated densities.^{50,51} The comparison of the present simulated D and η values with those reported in an earlier simulation study⁵³ is shown in Figure S2 (Section S1) of the Supporting Information. The comparison between the experimental^{4,52} and the current simulated diffusion and viscosity is presented in Section 3.

3. RESULTS AND DISCUSSION

3.1. Diffusion–Viscosity Decoupling. We calculate the self-diffusion coefficient D of the water molecules using the mean-square displacement (MSD) route $\lim_{t \rightarrow \infty} \langle |\Delta r(t)|^2 \rangle = 6Dt$. Here, the MSD $\langle |\Delta r(t)|^2 \rangle$ is calculated using the equation $\langle |\Delta r(t)|^2 \rangle = \langle |r_k(t) - r_k(0)|^2 \rangle$, where $r_k(t)$ and $r_k(0)$ are the positions of the k th water molecule at time t and time $t = 0$, respectively. Figure 1 presents MSD against

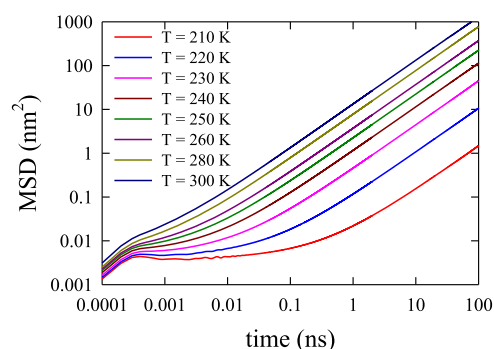


Figure 1. MSDs of water molecules as a function of time at different temperatures (210–300 K).

time at all eight different temperatures. The characteristic MSD plots at lower temperatures look similar to those for other supercooled liquids. The intermediate plateau region, occurring between the short-time ballistic part and the long-time diffusive part, is subdiffusive with fractional time dependence $\langle |\Delta r(t)|^2 \rangle \propto t^\alpha$; $0 < \alpha < 1$.⁵⁴ This subdiffusive part of MSD appears from the rattling of a molecule inside the solvent cage, while the former is momentarily trapped inside the cage.

Figure 2a presents the Arrhenius-type plot for simulated D values, calculated from the slope of the MSD plots at a long time, as a function of temperature. The simulated D values are in close agreement with the available experimental values.⁵² We have also compared in Figure S2 (Section S1) of the Supporting Information the present simulated D values with earlier simulated values.⁵³ Both the simulated and the experimental values are also listed in Table 2. (The error bar analysis for the diffusion coefficient has been detailed in Section S2 of the Supporting Information.) We found that above $T = 230$ K temperature, the simulated data fit quite well with the empirical Vogel–Fulcher–Tamman (VFT)-type relationship, $D = D_0 \exp[-B/(T - T_0)]$, where T is the temperature, T_0 is generally close to the glass-transition temperature, and D_0 and B are other fitting constants. We obtain the following fitting parameters after regressing the VFT equation onto the simulated D : $D_0 = 3.69 \times 10^{-4}$ cm²/s, $B = 364.05$ K, and $T_0 = 170.9$ K. These values are consistent with the experimental data.⁵²

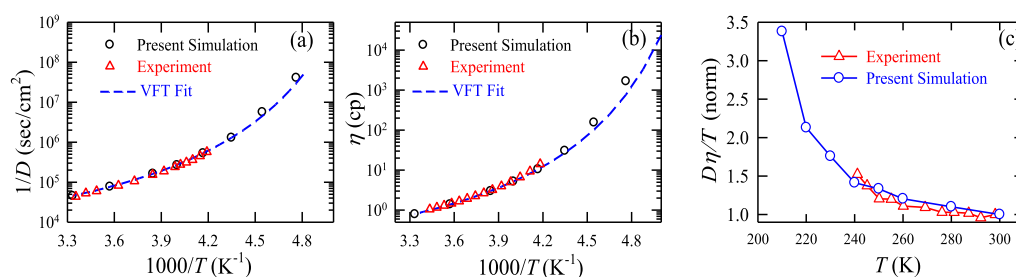


Figure 2. Comparison between the simulated and the experimentally measured transport coefficients.^{4,52} Arrhenius plots of simulated and measured translational diffusion coefficient D (a) and shear viscosity coefficient η (b). The simulated data are fitted with the VFT equation (blue dashed line) in both (a,b). (c) Temperature-dependent simulated and experimental⁴ $D\eta/T$ values. Both the theoretical and the experimental values are normalized to 300 K temperature.

Table 2. Comparison between the Simulated and the Experimental Parameters: Diffusion Coefficient (D), Viscosity Coefficient (η), and $D\eta/T$ ^a

T (K)	$D/10^{-5}$ ($D_{\infty}/10^{-5}$) (cm^2/s) simulation	$D/10^{-5}$ (cm^2/s) experiment	η (cp) simulation	η (cp) experiment	$D\eta/T/10^{-10}$ ($D_{\infty}\eta/T/10^{-10}$) ($\text{g cm s}^{-2} \text{K}^{-1}$) (simulation)	$D\eta/T/10^{-10}$ ($\text{g cm s}^{-2} \text{K}^{-1}$) (experiment)
210	0.0025 (0.0025)		1664		19.81 (19.81)	
220	0.0177 (0.0184)		155.1		12.48 (13.00)	
230	0.0773 (0.0813)		30.56		10.27 (10.77)	
240	0.1889 (0.2010)	0.204	10.52	12.68	8.280 (8.81)	10.80
250	0.3764 (0.4020)	0.385	5.194	5.392	7.820 (8.35)	8.300
260	0.6140 (0.6601)	0.650	2.990	3.059	7.060 (7.59)	7.650
280	1.2945 (1.4009)	1.440	1.396	1.425	6.450 (6.980)	7.330
300	2.2173 (2.4200)	2.300	0.793	0.892	5.861 (6.390)	6.840

^a D_{∞} and $D_{\infty}\eta/T$ values in the parentheses—listed in the second and sixth columns—are the corrected values of D and $D\eta/T$, respectively, for finite size effect.

Now, we calculate the viscosity coefficient η of water at different temperatures using the Green–Kubo relation via stress tensor correlation function. Figure 2b presents an Arrhenius plot of η as a function of temperature. Section S2 of the Supporting Information details the error bar analysis for the viscosity coefficient. The simulated η values match very well with both the experimentally measured⁴ and previously simulated^{25,26} η values at all the temperatures. See Figure S2b of the Supporting Information, where the present simulated η values are compared with earlier simulation.^{25,26} Table 2 summarizes both the simulated and the experimental η values.⁴ The visible agreement between the presented simulation and experimental η values validates the simulation force field and the protocols adopted in the present work. Above 230 K temperature, the simulated data fit quite well with the empirical VFT equation, $\eta = \eta_0 \exp[B/(T - T_0)]$; $\eta_0 = 4.21 \times 10^{-2}$ cp, $B = 378.4$ K, and $T_0 = 171.4$ K. However, the same equation does not fit very well with the simulated η values below 230 K temperature. However, we do not fit the Arrhenius equation only with the two temperatures: 210 and 220 K. Therefore, we cannot confirm the fragile-to-strong liquid transition^{55–59} below the 230 K temperature in the present study. It is worthwhile mentioning that in a recent study by Saito et al.,⁶⁰ the fragile-to-strong liquid transition has been observed for TIP4P/2005 water at 190 K temperature. Therefore, we do not expect the transition to be visible above 210 K temperature, the lowest temperature in our study.

We now check the validity of the SE relation using the present D and η values. The simulated and experimental $D\eta/T$ values for the whole temperature range are listed in Table 2. Figure 2c exhibits the normalized simulated and experimental $D\eta/T$ values as a function of temperature, which should be constant if the SE relation holds strictly. Note that the

experimental $D\eta/T$ values are obtained from the measured D ⁵² and η values.⁴ Normalization of the experimental and the simulated $D\eta/T$ values are done for the value at $T = 300$ K. It should be noted that the SE equation already breaks down at 300 K temperature. However, normalization of the $D\eta/T$ values to 300 K temperature does not result in a serious error in the calculation because the breakdown of the SE equation is not much intense at 300 K temperature.^{2,4} Figure 2c clearly shows the gradual deviation of the normalized simulated $D\eta/T$ from unity as the temperature decreases from the room temperature. This indicates an increasing violation of the SE equation—which reaches $\sim 80\%$ —on cooling down the system to 210 K. This is consistent with the available experimental result.⁴ Another parameter for quantifying the agreement between the simulated and experimentally measured $D\eta/T$ values is the phenomenological exponent ω , which can be calculated by fitting with the equation, $D \propto \eta^{-1+\omega}$.^{9,61–64} We obtain the value of $\omega = 0.12$. For hard spheres and other similar model liquids, $\omega = 0.22$ ⁶¹ in the SE equation breakdown regime. For confined water, the value of $\omega = 0.23$, which was calculated via the equation $D \propto T^{-1+\omega}$.² The experiment by Dehaoui et al.⁴ showed that the fitting of the data using $D \propto (\eta/T)^{\xi}$ gives the value of $\xi = -1$ at high temperature ($T > 350$ K) and $\xi = -0.8$ at low temperature ($T < 350$ K). Fitting of our simulated data with the above equation gives $\xi = -0.85$. Interestingly, the study of Mallamace et al.⁶⁵ suggested a putative universal crossover of ξ from -1 to -0.85 upon cooling for nine different glass-forming liquids. Therefore, our simulated SE breakdown parameters are in close agreement with the experimental ones.

Although 2000 water molecules (sufficiently large system size) are considered in the present simulation, the simulated D values may still suffer from finite size effect because of the

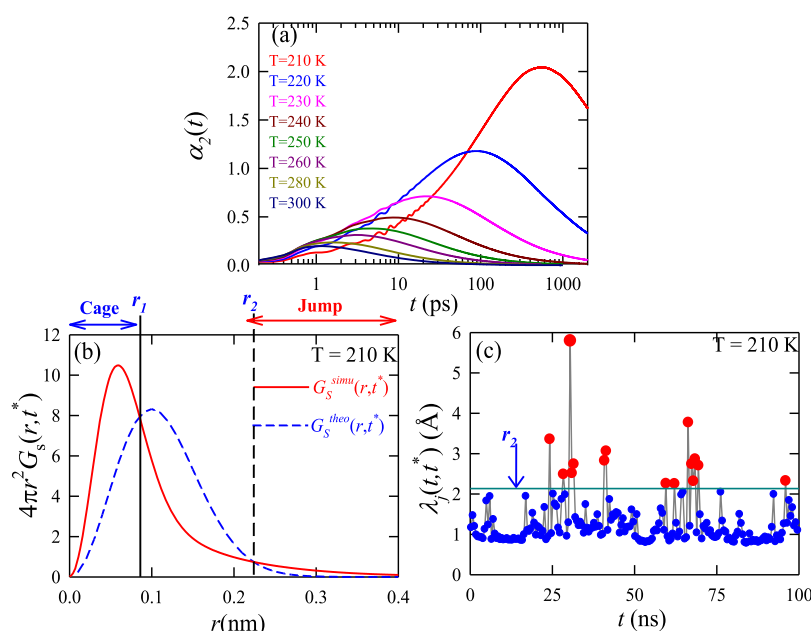


Figure 3. (a) Non-Gaussian parameter $\alpha_2(t)$ as a function of time for all the temperatures studied. Times t^* of $\alpha_2(t)$ maxima are listed in Table 3. (b) The self-part of the van Hove correlation functions $G_s^{\text{simu}}(r, t^*)$ (solid line) and the corresponding ideal Gaussian distribution ($G_s^{\text{theo}}(r, t^*)$) (dashed line) at time t^* , when $\alpha_2(t)$ is maximum at $T = 210$ K. The similar plots for other temperatures are presented in Figure S3 of the Supporting Information. (c) Distance traversed by one water molecule, $\lambda_j(t, t^*)$, in the j th trajectory segment. The horizontal line indicates the cutoff distance r_2 . The red circles, which are above the cutoff distance r_2 , represent the jump trajectory segments.

hydrodynamic interactions between periodic images of the simulation boxes. Therefore, we correct the D values from system size effects. It has been found in theoretical studies that for an infinite liquid, the self-diffusion coefficient D_∞ can be obtained using the equation^{54,66,67} $D_\infty = D + 2.837k_B T / 6\pi\eta L$. Here, D is the self-diffusion coefficient without the correction (as reported in Table 2), k_B is the Boltzmann constant, T is the temperature, η is the viscosity of the medium, and L is the simulation box length. The calculated D_∞ values are listed in Table 2, where the D_∞ values are only slightly different from D . This indicates that 2000 water molecules constitute a sufficiently large system size. We have also calculated the system size corrected $D_\infty\eta/T$ values for different temperatures. The $D_\infty\eta/T$ values are also listed in Table 2. As expected, $D_\infty\eta/T$ and $D\eta/T$ values are very close to each other.

Last, Figure 2 and Table 2 clearly show that neither the experiment nor the present simulation shows abrupt changes in diffusion coefficient D , viscosity coefficient η , and $D\eta/T$ as the temperature crosses the simulated Widom line (obtained for TIP4P/2005 water)⁶⁸ at $T \approx 230$ K for 1 bar pressure. This is consistent with an earlier simulation study for the E3B3 water model.^{69,70} However, simulation studies at higher pressures suggested that the diffusion coefficient shows an abrupt change near the Widom line only if the pressure is closer to the theoretical LLCF.^{69,70} Therefore, the key reason for not predicting the rapid changes in diffusion coefficient D , viscosity coefficient η , and $D\eta/T$ by the present simulation is mainly the consideration of 1 bar pressure, which is much less than the simulated critical pressure for TIP4P/2005 water ($T = 193$ K, $p = 1350$ bar).⁶⁸

3.2. Analysis of Jump Diffusion. Now, we turn our focus on the quantitative jump analysis for estimating the jump diffusion coefficient D_{jump} of the water molecules at all the simulated temperatures. One of the most crucial steps of the analysis is the correct identification of a translational jump

occurrence. The most straightforward method of identifying a jump occurrence is via calculating the displacement of a molecule from its position at the beginning of the trajectory $t = 0$.^{24,71–75} Despite the simplicity of the method, this approach fails in the quantitative analysis of jump diffusion coefficient because of the following reason. This method correctly identifies only those jumps, where the initial and the final positions—the initial position is the position of the molecule just before the jump occurrence and the final position refers to the new position of the molecule after the jump occurrence—of the jumping molecule are collinear with the position at $t = 0$. The inaccuracies of identification of the jump occurrence and estimation of the jump length are very high when the above three coordinates deviate from linearity.²⁴ The method completely loses its hold when the three coordinates form a right angle triangle. In that case, the jump displacement shows either no peak at all or a very small peak with an intensity too low to detect among the thermal noise. This method, therefore, underestimates the contribution of jump diffusion to the overall diffusion.²⁴ A more quantitative method is, therefore, indispensable.

A quantitative method³⁸ was used earlier to estimate the jump diffusion of a model glass-forming liquid. The algorithm is based on the understanding that the fluctuation of a caged particle's position from the average position on a given time scale is of the order of the Debye–Waller (DW) factor. Therefore, this method considers a particle as a jumping one, which has the fluctuation higher than the DW factor. The caged particles are those which have lower fluctuations than the DW factor. This method successfully estimated a single particle's jump diffusion coefficient, which was eventually utilized to calculate the diffusion constant of the glass-forming liquid. However, it is not clear whether the jump diffusion coefficient—obtained from the above method—is only due to

large amplitude displacements, which are responsible for the breakdown of the SE equation in the supercooled liquid.

An alternative method,¹³ based on oscillator model theory (first applied in understanding particle diffusion through a cylindrical nanopore),⁷⁶ was used to calculate the jump diffusion coefficient (neck diffusion) of a small solute particle in a viscous liquid. This method successfully captured the importance of jump diffusion of particles in a glass-forming liquid. However, it is not clear whether these methods are applicable for estimating the jump diffusion coefficient of a bigger solute or solvent in a more complex environment.

We have used here a different method, which is based on the technique, previously developed by Raptis et al.^{77,78} and later modified by Araque et al.⁷⁹ This method basically examined the radii of gyration $R_g(t, \Delta t)$ of different segments of the molecular trajectories in a three-dimensional positional coordinate space. $R_g(t, \Delta t)$ for the particular trajectory segment of length Δt (or n number of time steps) is calculated using the following equation.

$$R_g(t, \Delta t) = \sqrt{\frac{1}{n} \sum_{i=1}^n [r_i(t; \Delta t) - r_{CM}(t; \Delta t)]^2} \quad (1)$$

In eq 1, $r_i(t; \Delta t)$ and $r_{CM}(t; \Delta t)$ are, respectively, the position of one molecule at the i th time frame and the center of mass of the trajectory segment of length Δt . $r_{CM}(t; \Delta t)$ is calculated by the following equation.

$$r_{CM}(t, \Delta t) = \frac{1}{n} \sum_{i=1}^n r_i(t; \Delta t) \quad (2)$$

As the diffusion of the water molecules increases with the temperature, consideration of the same Δt for all the temperatures can lead to unreasonable results. For example, $\Delta t = 10$ ps trajectory segment at 210 K temperature spreads in much smaller space than that at 300 K. In order to avoid this apparent inconsistency, we choose different Δt for different temperatures. It is observed that consideration of Δt as the characteristic time t^* —when the non-Gaussian parameter $\alpha_2(t)$ is maximum—works perfectly well under any situation.⁵⁸ We calculate $\alpha_2(t)$ using the following equation

$$\alpha_2(t) = 3\langle r^4(t) \rangle / 5\langle r^2(t)^2 \rangle - 1 \quad (3)$$

where $\langle r^2(t) \rangle$ is the MSD of the k th molecule $\langle r^2(t) \rangle = \langle |r_k(t) - r_k(0)|^2 \rangle$ and $\langle r^4(t) \rangle$ is written as $\langle r^4(t) \rangle = \langle |r_k(t) - r_k(0)|^4 \rangle$. However, we have also checked the dependence of Δt value on the result and found that a change of Δt value by a maximum 30% does not appreciably change the results. The above analysis has been described in Section S3 of the [Supporting Information](#). Also, the peak of $\alpha_2(t)$ corresponds to the highest heterogeneous dynamics of the molecules at time t^* .^{80,81}

Figure 3a presents $\alpha_2(t)$ against time in the current range of temperatures ($T = 210$ – 300 K). The peak intensity of $\alpha_2(t)$ increases with decreasing temperature. This indicates an increase of dynamical heterogeneity because of the decrease in temperature. Also, the t^* value, listed in Table 3, increases from ~ 1 to ~ 560 ps on decreasing the temperature from $T = 300$ to 210 K. Therefore, the required length Δt of the trajectory segment—the input of eqs 1 and 2—increases with decreasing temperature.

We divide the trajectories of each water molecule into multiple segments each of length t^* . We calculate $R_g(t, t^*)$ for all the trajectory segments. The distance traversed by one

Table 3. Temperature-Dependent Time Scale t^* —at Which the Non-Gaussian Parameter $\alpha_2(t)$ Is the Maximum—and the Crossing Distances between Simulated and Theoretical Self-Part of the van Hove Correlation Functions

T (K)	t^* (ps)	r_1 (nm)	r_2 (nm)
210	560	0.086	0.215
220	88.6	0.092	0.230
230	22.0	0.098	0.225
240	9.00	0.104	0.240
250	4.30	0.105	0.245
260	3.00	0.111	0.260
280	1.60	0.115	0.270
300	1.10	0.120	0.300

water molecule in the j th trajectory segment of t^* length is $\lambda_j(t, t^*)$, which can be calculated using the following formula^{77–79}

$$\lambda_j(t, t^*) = 2R_g(t, t^*) \quad (4)$$

We note that the translational jump occurrences are not ubiquitous in all these trajectory segments. At this point, we employ an efficient method to identify the translational jump segments correctly. The method⁷⁹ uses the self-part of the van Hove correlation function $G_S^{\text{simu}}(r, \Delta t)$, which is calculated using the following equation^{80,81}

$$G_S^{\text{simu}}(r, \Delta t) = \frac{1}{N_w} \left\langle \sum_{k=1}^{N_w} \delta(r - |r_k(t_0) - r_k(t_0 + \Delta t)|) \right\rangle_{t_0} \quad (5)$$

In eq 5, $r_k(t_0)$ is the position of the k th molecule at t_0 time, $r_k(t_0 + \Delta t)$ is the position of the same particle at $t_0 + \Delta t$ time, and N_w is the total number of water molecules. $G_S^{\text{simu}}(r, \Delta t)$ is averaged over both N_w and all possible initial t_0 times. The deviation of $G_S^{\text{simu}}(r, \Delta t)$ from the Gaussianity ($G_S^{\text{theo}}(r, \Delta t) = [3/2\pi\langle r^2(\Delta t) \rangle]^{3/2} \exp[-3r^2/2\langle r^2(\Delta t) \rangle]$)^{80,81} is maximum at time $\Delta t = t^*$. Both the $G_S^{\text{simu}}(r, t^*)$ and $G_S^{\text{theo}}(r, t^*)$ are plotted in Figure 3b for $T = 210$ K and in Figure S3 of the [Supporting Information](#) for all the temperatures. $G_S^{\text{simu}}(r, t^*)$ crosses $G_S^{\text{theo}}(r, t^*)$ at two characteristic r values, r_1 and r_2 , by which we define the cage and the jump trajectories, respectively. At the smaller r limit ($r < r_1$), the actual displacements of the water molecules are less than the expected value obtained from $G_S^{\text{theo}}(r, t^*)$. Therefore, the j th trajectory segment of length $\lambda_j(t, t^*) < r_1$ is a cage trajectory. On the other hand, at a larger r limit ($r > r_2$), the actual displacement of the water molecule is larger than the displacement predicted by $G_S^{\text{theo}}(r, t^*)$. Table 3 presents the numerical values of r_1 and r_2 for the different temperatures. Therefore, the trajectory segments, where the distance traversed by the molecule $\lambda_j(t, t^*) > r_2$, is categorized as the jump trajectory.⁷⁹

Before moving forward, we make an important point. For characterizing a jump trajectory segment, we have adopted the above method, which is also detailed in ref 79. The key difference between the present method and the method by Raptis et al.^{77,78} is as follows. In both the methods, $\lambda_j(t, \Delta t)$ is calculated by eq 4. However, there is one issue regarding the correct identification of the peaks (out of all the peaks of $\lambda_j(t, \Delta t)$ plotted as a function of t), which are responsible for the actual jump. In order to resolve the issue, the method by Raptis et al. used a weighted jump length. Therefore, slightly big jumps contribute less to the total diffusion. This method,

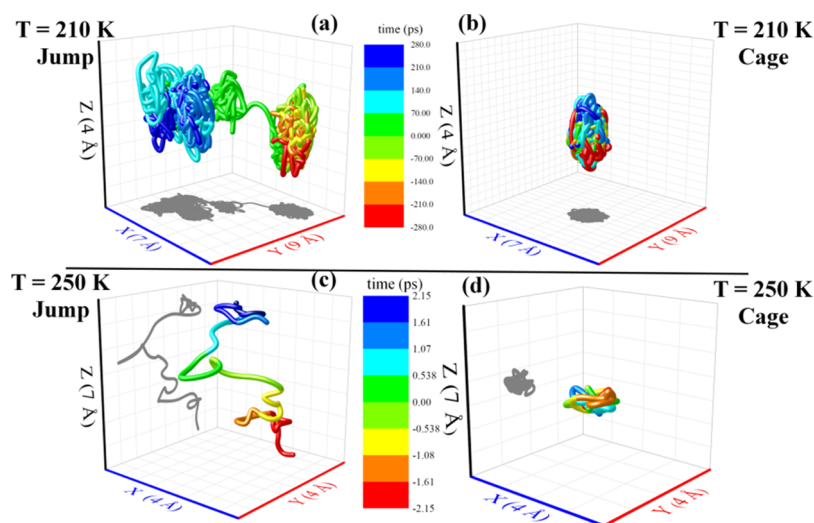


Figure 4. Four representative jump and cage trajectories of length t^* for one water molecule at two representative temperatures: 210 K (top panels) and 250 K (bottom panels). The color-mapping denotes the direction of the time evolution of a trajectory.

therefore, considers all the peaks of the weighted $\lambda_i(t, \Delta t)$ as “jumps”. The definition of jump translation is therefore slightly confusing. On the other hand, the present method⁷⁹ uses eq 4 only (without using the weighted parameter) to calculate $\lambda_j(t, \Delta t)$ and distinguish a trajectory segment as the “jump” only when it meets the criteria, $\lambda_j(t, \Delta t) > r_2$, where r_2 is the second crossing point between $G_S^{\text{simu}}(r, \Delta t)$ and $G_S^{\text{theo}}(r, \Delta t)$. The fact that $G_S^{\text{simu}}(r, \Delta t)$ deviates $G_S^{\text{theo}}(r, \Delta t)$ at the most for $\Delta t = t^*$ (t^* is the time when $\alpha_2(t)$ is maximum) makes t^* the absolute choice for Δt . Clearly, the present method is in accordance with the classical picture of the jump translation, which is believed to have emerged from the spatio-temporal heterogeneity of the medium, the time scale of which can be quantified by t^* and the deviation of $G_S^{\text{simu}}(r, \Delta t)$ from $G_S^{\text{theo}}(r, \Delta t)$.^{80,81} In a recent article,²⁴ two of the authors have shown that the jump diffusion of a solute in the supercooled water emanates from dynamic heterogeneity of the medium via correlated translational/rotational solvent dynamics. Interestingly, the approximate jump analysis in ref 24, via visual identification of large sudden jumps, provided similar results to the present work. This validates the method of identification of a jump occurrence in the present work.

Figure 3c exhibits an example of $\lambda_j(t, t^*)$ as a function of time for one water molecule at $T = 210$ K temperature as a representative temperature. A peak, whose intensity crosses the distance r_2 , represents a translational jump trajectory. Conversely, we characterize a trajectory segment as the cage trajectory, which has $\lambda_j(t, t^*)$ value less than the cutoff r_1 . Here, the cage trajectory refers to the rattling motion of a molecule inside the solvent cage plus the overall translation of the whole solvent cage with the tagged molecule in the center. Figures 4 and S4 of the Supporting Information present several examples of the cage and jump trajectory segments. It is evident from the representative examples that the above protocol for identifying the jump and cage trajectories is working as expected because the identified jump trajectory segments consist of sudden change(s) of the position of the molecule in between initial cage to final cage and identified cage trajectory segments are actually rattling trajectories.

As we have correctly identified the jump trajectory segments, we now calculate the jump diffusion coefficient D_{Jump} using the following equation^{77–79}

$$D_{\text{Jump}} = \frac{1}{6} \nu_{\text{Jump}} \lambda_{\text{Jump}}^2 \quad (6)$$

ν_{Jump} is the frequency of the translational jump occurrence of one water molecule. ν_{Jump} is calculated using the following equation

$$\nu_{\text{Jump}} = \frac{n_{\text{Jump}}}{n_w t_{\text{traj}}} \quad (7)$$

λ_{Jump}^2 is the average square jump length, which is obtained by averaging $\lambda_j^2(t, t^*)$ over the number of jump occurrences n_{Jump} in the entire system using the following equation

$$\lambda_{\text{Jump}}^2 = \lim_{n_{\text{Jump}} \rightarrow \infty} \frac{1}{n_{\text{Jump}}} \sum_{j=1}^{n_{\text{Jump}}} \lambda_j^2(t, t^*)|_{\text{for } \lambda_j(t, t^*) > r_2} \quad (8)$$

Note that eq 6 can be obtained from the random walk problem. Because a jumping water molecule can travel a distance λ_j in any random directions, and these jumps are statistically independent of each other, the current problem effectively turns into the random walk problem. The derivation of eq 6 has been presented in Section S4 of the Supporting Information.

We have listed, in Table 4, the numerical values of n_{Jump} , ν_{Jump} , λ_{Jump}^2 , and the percentage of jump trajectory segments, $P_{\text{Jump}} = \frac{n_{\text{Jump}}}{n_w t_{\text{traj}} / t^*} \times 100$ (the values of t_{traj} are presented in Table 1) for different temperatures. Using the above numerical values in eq 6, we calculate D_{Jump} of the water molecules at all the temperatures. The values are listed in Table 5.

Figure 5a exhibits the percentage contribution of D_{Jump} to the overall diffusion D of the water molecules $100(D_{\text{Jump}}/D)\%$ as a function of temperature. The contribution increases with decreasing temperature and reaches approximately 50% at $T = 210$ K. On the other hand, the percentage of jump trajectory segments P_{Jump} increases from $\sim 0.12\%$ of the total trajectory segments at $T = 300$ K to slightly more than 5% at $T = 210$ K. Therefore, approximately 1 jump in 20 trajectory segments contributes 50% of the overall diffusion of the water molecules at 210 K temperature. In other words, a small fraction of the jump trajectory contributes to a large fraction of the overall diffusion at $T = 210$ K.

Table 4. Average Number of Jump (n_{jump}), Jump Frequency (ν_{jump}), Average Jump Displacement (λ_{jump}^2), and the Percentage of the Jump Trajectory Segment (P_{jump}) at Different Temperatures

T (K)	n_{jump}	jump frequency ν_{jump} (ns^{-1})	λ_{jump}^2 (\AA^2)	percentage of jump trajectory segment $P_{\text{jump}} = \frac{n_{\text{jump}}}{n_{\text{wt}} t_{\text{traj}} / t^*} \times 100$
210	93 000	0.093	8.12	5.21
220	487 894	0.488	8.01	4.32
230	1 418 488	1.773	7.13	3.90
240	1 843 861	2.305	7.62	2.07
250	1 631 136	2.719	7.67	1.17
260	1 040 193	2.600	8.47	0.78
280	529 883	2.649	8.94	0.42
300	213 386	1.067	10.6	0.12

We now check the validity of the SE equation using the calculated D_{jump} and the simulated η of the medium. Table 5 lists $D_{\text{jump}}\eta/T$ at different temperatures. Figure 5b displays the normalized $D_{\text{jump}}\eta/T$ values as a function of time where we see that $D_{\text{jump}}\eta/T$ increases rapidly with decreasing temperature. The value of the latter increases by ~ 200 times as the temperature is decreased from $T = 300$ to 210 K. Therefore, as expected, D_{jump} is completely decoupled from the viscosity almost at all the temperatures. This is expected because the SE equation was not developed for large displacement but only for the small step diffusive process. It is evident from Figure 5 that similar to D and η , abrupt change of D_{jump} is also not observed as the temperature crosses ~ 230 K temperature (the position of the Widom line for TIP4P/2005 water at 1 bar). This is again due to the lower simulated pressure (1 bar) condition in the present case than the simulated critical pressure for TIP4P/2005 water ($T = 193$ K, $p = 1350$ bar).⁶⁸

Note that D_{jump} has been calculated by considering only the large amplitude displacements ($\lambda_j(t, t^*) > r_2$) of the water molecules. In other words, D_{jump} is that component of the total diffusion D , which considers only some long step displacements. Therefore, we can write the total diffusion coefficient D as a sum of two components. The first component D_{jump} comes from the jump translation exclusively. On the other hand, the smaller step displacements collectively can give rise to another diffusion coefficient. We call it residual diffusion coefficient D_{Res} , which can be calculated from the following equation

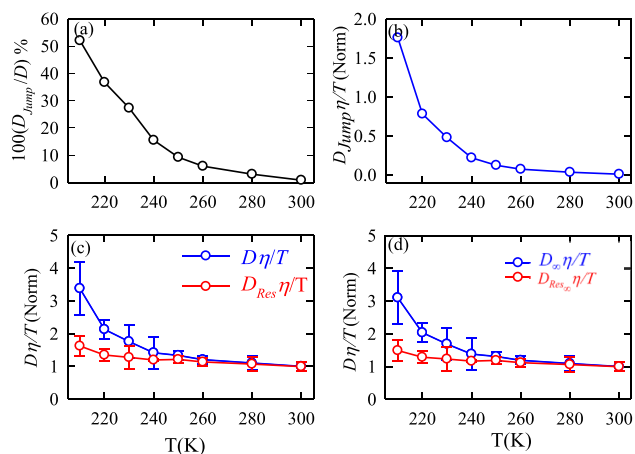


Figure 5. (a) Percentage contribution of the jump diffusion coefficient D_{jump} to the total diffusion coefficient D of the water molecules as a function of temperature. Temperature-dependent coupling of viscosity with (b) translational jump diffusion coefficient D_{jump} , (c) overall translational diffusion coefficient D and the residual diffusion coefficient D_{Res} ($D - D_{\text{jump}}$), and (d) system size effect corrected diffusion value D_{∞} and $D_{\text{Res},\infty}$ ($D_{\infty} - D_{\text{jump},\infty}$). The error bars of $D\eta/T$ in (c,d) are the standard errors. (See Section S2 of the Supporting Information for details of error analysis.)

$$D_{\text{Res}} = D - D_{\text{jump}} \quad (9)$$

Note that similar decompositions of the total diffusion coefficient are ubiquitous in the literature, although in different aspects. The total diffusion coefficient of a small solute particle in the molecular glass-forming liquid was written as a sum of neck diffusion (analogous to D_{jump}) and the diffusion coefficient emanating from the SE equation.¹³ Therefore, the physical meaning of D_{Res} relies on the correct identification of the jump trajectory segments because the rest of the trajectory segments contribute to D_{Res} . Therefore, D_{Res} is that component of D , which completely excludes molecular jump translation and which emanates from the small step diffusion process as in standard Einstein's Brownian motion. This immediately suggests that D_{Res} should be coupled to the viscosity of the medium and thereby follows the SE equation.

We have calculated D_{Res} for all the temperatures and listed their numerical values in Table 5. We now check the validity of the SE equation by checking the effect of the temperature on the numerical value of $D_{\text{Res}}\eta/T$, which are presented in Table

Table 5. Different Components of Diffusion Coefficients: Diffusion Coefficient Due to Jump (D_{jump}) and Residual Diffusion (D_{Res}) of the Water Molecules, the Percentage Contribution of D_{jump} to Total Diffusion Coefficient D , $D_{\text{jump}}\eta/T$ Values, and the $D_{\text{Res}}\eta/T$ at Eight Different Temperatures^a

T (K)	$D_{\text{jump}}/10^{-5}$ ($D_{\text{jump},\infty}/10^{-5}$) (cm^2/s)	$D_{\text{Res}}/10^{-5}$ ($D_{\text{Res},\infty}/10^{-5}$) (cm^2/s)	100 (D_{jump}/D)%	$D_{\text{jump}}\eta/T/10^{-10}$ ($D_{\text{jump},\infty}\eta/T/10^{-10}$) ($\text{g cm s}^{-2} \text{K}^{-1}$)	$D_{\text{Res}}\eta/T/10^{-10}$ ($D_{\text{Res},\infty}\eta/T/10^{-10}$) ($\text{g cm s}^{-2} \text{K}^{-1}$)
210	0.0013 (0.0013)	0.0012 (0.0012)	52.00	10.301 (10.301)	9.5086 (9.5086)
220	0.0065 (0.0068)	0.0112 (0.0116)	36.72	4.5825 (4.7635)	7.8960 (8.2085)
230	0.0211 (0.0222)	0.0562 (0.0591)	27.30	2.8035 (2.9485)	7.4673 (7.8538)
240	0.0293 (0.0312)	0.1596 (0.1698)	15.51	1.2843 (1.3666)	6.9958 (7.4439)
250	0.0348 (0.0372)	0.3416 (0.3648)	9.245	0.7230 (0.7722)	7.0971 (7.5798)
260	0.0368 (0.0396)	0.5772 (0.6205)	5.993	0.4232 (0.4550)	6.6378 (7.1362)
280	0.0394 (0.0426)	1.2551 (1.3583)	3.044	0.1964 (0.2126)	6.2576 (6.7719)
300	0.0189 (0.0206)	2.1984 (2.3994)	0.852	0.0500 (0.0545)	5.8111 (6.3423)

^aThe values in parenthesis are the finite size effect corrected values of the jump diffusion coefficients $D_{\text{jump},\infty}$ (second column), the residual diffusion coefficients $D_{\text{Res},\infty}$ (third column), $D_{\text{jump}}\eta/T$ (fifth column), and $D_{\text{Res},\infty}\eta/T$ (sixth column).

Table 6. Effect of the Jump (D_{Jump}), Residual Diffusion (D_{Res}), and $D_{\text{Res}}\eta/T$ on the 10% Change of r_2 Second Crossing Distance Between $G_{\text{S}}^{\text{simu}}(r, \Delta t)$ and $G_{\text{S}}^{\text{theo}}(r, \Delta t)$ at Eight Different Temperatures^a

T (K)	r_2 (Å)	ν_{jump} (ns ⁻¹)	λ_{jump}^2 (Å ²)	$D_{\text{Jump}}/10^{-5}$ cm ² /s	$D_{\text{Res}}/10^{-5}$ cm ² /s	$D_{\text{Res}}\eta/T/10^{-10}$ cm ² /s
210	$r_2 - 10\%$	0.132	6.95	0.0015	0.0010	7.9238
	r_2	0.093	8.12	0.0013	0.0012	9.5086
	$r_2 + 10\%$	0.066	9.36	0.0010	0.0015	11.886
220	$r_2 - 10\%$	0.775	6.81	0.0088	0.0089	6.2745
	r_2	0.488	8.01	0.0065	0.0112	7.8960
	$r_2 + 10\%$	0.307	9.36	0.0048	0.0129	9.0945
230	$r_2 - 10\%$	3.116	6.00	0.0312	0.0461	6.1253
	r_2	1.773	7.13	0.0211	0.0562	7.4673
	$r_2 + 10\%$	1.004	8.41	0.0140	0.0633	8.4106
240	$r_2 - 10\%$	4.631	6.40	0.0493	0.1396	6.1191
	r_2	2.305	7.62	0.0293	0.1596	6.9958
	$r_2 + 10\%$	1.140	9.00	0.0171	0.1718	7.5306
250	$r_2 - 10\%$	6.064	6.40	0.0650	0.3114	6.4696
	r_2	2.719	7.67	0.0348	0.3416	7.0971
	$r_2 + 10\%$	1.216	9.12	0.0185	0.3579	7.4357
260	$r_2 - 10\%$	6.195	7.08	0.0731	0.5409	6.2204
	r_2	2.600	8.47	0.0368	0.5772	6.6378
	$r_2 + 10\%$	1.088	10.0	0.0183	0.5957	6.8506
280	$r_2 - 10\%$	6.912	7.40	0.0854	1.2091	6.0282
	r_2	2.649	8.94	0.0394	1.2551	6.2576
	$r_2 + 10\%$	0.999	10.6	0.0176	1.2769	6.3663
300	$r_2 - 10\%$	3.342	8.82	0.0492	2.1681	5.7310
	r_2	1.067	10.6	0.0189	2.1984	5.8111
	$r_2 + 10\%$	0.329	12.7	0.0069	2.2104	5.8428

^aWe also compared the jump frequency and average square jump length for all eight temperatures.

5. Figure 5c plots the normalized $D_{\text{Res}}\eta/T$ as a function of temperature. Note that the normalization has been done with respect to the value at $T = 300$ K temperature. Very interestingly, unlike the $D\eta/T$, which continuously increases with decreasing temperature, the $D_{\text{Res}}\eta/T$ value remains almost constant.^{1–4} This indicates that once the translational jump only diffusion is separated out from the overall diffusion, the residual diffusion perfectly couples with the viscosity and thus follows the SE equation. Therefore, the jump diffusion of the molecules is the fundamental origin for the observed decoupling of the molecular diffusion from the viscosity of the medium. This is one of the key results of this work as it categorically proves the concept that the origin of the well-known diffusion–viscosity decoupling in supercooled water (liquid) is the translational jump diffusion of molecules. Two of us have previously shown the mechanism of these translational jumps in great details and the crucial role of the synchronization between the translational and the rotational motion of the solvent water molecules for inducing these jump events.^{24,75}

Similar to the correction of the system size effect for D values, listed in Table 5, we also correct the D_{Jump} and D_{Res} values for infinite liquid. For this, we have scaled the values of D_{Jump} and D_{Res} by the same correction factor D_{∞}/D . The corrected $D_{\text{Jump}\infty}$ and $D_{\text{Res}\infty}$ are listed in Table 5. Figure 5d plots the normalized $D_{\text{Res}\infty}\eta/T$ as a function of temperature, where the normalization is done for the $D_{\infty}\eta/T$ value at $T = 300$ K temperature. Similar to the normalized $D_{\text{Res}}\eta/T$ value, the normalized $D_{\text{Res}\infty}\eta/T$ remains almost constant except a slight increase at 210 K, which may come from larger error at that temperature.^{1–4}

Last, before concluding, we discuss a couple of important points. First, we discuss how the key results of the present work—mainly the D_{Jump} values—are affected by various input parameters and jump criteria. As we consider a trajectory segment as a jump one if $\lambda_i(t, t^*) > r_2$. Therefore, D_{Jump} must depend on the r_2 value. However, the r_2 value is not an independent parameter but the second crossing distance between $G_{\text{S}}^{\text{simu}}(r, \Delta t)$ and $G_{\text{S}}^{\text{theo}}(r, \Delta t)$, which are actually dependent on the Δt value. Therefore, the only input parameter in the jump analysis is the numerical value of Δt . Once we choose the Δt value, the criterion for the jump motion is already set. In the present study, we have considered Δt value as the time (t^*) at which the $\alpha_2(t)$ is maximum. The above consideration of t^* as Δt is as per the previous work by Araque et al (ref 79 of the MS). This can also be justified from the fact that t^* is the time when the displacement distribution of molecules becomes substantially non-Gaussian in nature. Therefore, at time t^* , the dynamics of the molecules are heterogeneous at the most. However, one can check the effect of Δt value on the results, particularly D_{Jump} . We have varied the Δt value ranging from $0.7t^*$ (30% less than t^*) to $1.3t^*$ (30% more than t^*) in a regular interval of $0.1t^*$ (10% of t^*) and performed the complete jump analysis for each of them. The results are presented in Figure S7 of the Supporting Information. We see that the change is nominal if the Δt value is increased/decreased by 30% from the t^* value. Therefore, the present method is not very much dependent on the choice of the Δt value until it is not changed by a very large extent.

Now, we discuss the effect of the r_2 value on the key results of the present work. Evidently, D_{Jump} must depend on the r_2 value. Note that the r_2 value is not an independent parameter but actually determined by the second crossing distance between $G_{\text{S}}^{\text{simu}}(r, \Delta t)$ and $G_{\text{S}}^{\text{theo}}(r, \Delta t)$, which finally depend on

the Δt value. However, one may ask the effect of the results on the subtle deviation of r_2 value, which may arise due to small error of the $G_S^{\text{simu}}(r, \Delta t)$. This is particularly important for the higher temperatures, when the second crossing point between $G_S^{\text{simu}}(r, \Delta t)$ and $G_S^{\text{theo}}(r, \Delta t)$ is not sharp. Therefore, we check the dependence of $D_{\text{Res}}\eta/T$ on a slight variation of the r_2 value. We calculated the $D_{\text{Res}}\eta/T$ with the r_2 values changed 10% from the original data, reported in Table 3. We have summarized the results in Table 6. The results suggest that the key result $D_{\text{Res}}\eta/T$ is not changed appreciably, particularly at the higher temperature, even though various quantities (such as ν_{Jump} , λ_{Jump}^2 , D_{Jump} , and so forth) are slightly affected. This is because the contribution of D_{Jump} to the total diffusion is much less significant at high temperature.

Finally, we discuss a very crucial point. Even though eq 6 can be derived from the random walk problem—described in Section S4 of the Supporting Information—one can still question the validity of the equation in the present system where the solvent is spatiotemporally heterogeneous at the supercooled region. Also, eq 9 has been written on the justification that while the D_{Jump} emanates from the large amplitude jump motion of the water molecules, the smaller step displacements collectively can give rise to another diffusion coefficient, D_{Res} . Therefore, the total diffusion coefficient is decomposed into two components: D_{Jump} and D_{Res} . We validate the above point by evaluating D_{Jump} and D_{Res} independently using the MSD route instead of using eqs 6–9. For this, we separate the full trajectory into two parts: the trajectory portion containing only the jump events and the leftover portion of the trajectory containing only smaller step displacements. The conditions, which set the criteria for the jump and the smaller step trajectory segments, are $\lambda_j(t, t^*) > r_2$ and $\lambda_j(t, t^*) < r_2$, respectively. Now, because the number of jump trajectory segments is much less than the residual trajectory segments, visible from Table 4, presumably most of the times two successive jump trajectory segments are separated by one or more residual trajectory segment(s). This introduces discontinuity of the jump trajectory, which gives erroneous D_{Jump} value. To solve this issue, we have connected the last point of one jump trajectory with the first point of the next jump trajectory segment such that they are separated by time. Therefore, during the extraction of the jump trajectory from the original trajectory, the residual trajectory segments are replaced by the same phase space variables of the last point of the previous jump trajectory segment. Thus, during the residual trajectory segments, the particle is at rest. By this way, we take the jump frequency into account. We extract the pure residual trajectory in the same way as above, but this time during the jump trajectory segments the particle is at rest. Now, we calculate the MSDs from the above two trajectories (jump and the residual) separately using the following equations

$$\text{MSD}_{\text{Jump}} = \langle |\Delta r(t)|^2 \rangle = \langle |\mathbf{r}_k(t) - \mathbf{r}_k(0)|^2 \rangle_{\text{for } \lambda_j(t, t^*) > r_2} \quad (10)$$

$$\text{MSD}_{\text{Res}} = \langle |\Delta r(t)|^2 \rangle = \langle |\mathbf{r}_k(t) - \mathbf{r}_k(0)|^2 \rangle_{\text{for } \lambda_j(t, t^*) < r_2} \quad (11)$$

Here, $\mathbf{r}_k(t)$ and $\mathbf{r}_k(0)$ are the positions of the k th water molecule at time t and time $t = 0$, respectively. Therefore, the MSD_{Jump} is calculated only for the jump trajectory segments, set by the criteria $\lambda_j(t, t^*) > r_2$ (for the j th trajectory segment of the k th particle). If a residual jump trajectory segment comes

in between two jump trajectory segments, the displacement does not add up. The same is true for calculating the MSD_{Res} using eq 11.

The jump, the residual, and the total MSD plots are presented in Figure S8 for three representative temperatures. Clearly, both the jump and the residual MSD components are linearly proportional to the time. To get the D_{Jump} and D_{Res} values, we calculate the slopes of the jump and the residual MSDs at a long time and compare with the values obtained via eqs 6–9 for all the temperatures in Table S2 of the Supporting Information. The values obtained from the MSD route are in very close agreement with the values calculated using eqs 6–9. With the above D_{Jump} and D_{Res} values, we have plotted in Figure S9 of the Supporting Information the percentage contribution of the D_{Jump} to the overall diffusion D of the water molecules $100(D_{\text{Jump}}/D)\%$, $D_{\text{Jump}}\eta/T$, and $D_{\text{Res}}\eta/T$ at different temperatures and compared them with the data (obtained from eqs 6–9) already presented in Figure 5a–c. Clearly, the results are in close agreement with each other. This further emboldens the validity of eqs 6–9 and the physical significance of the D_{Res} , which emanates from the collective small step displacements of the water molecules. An even closer agreement of the results at lower temperatures may be found by analyzing a longer production trajectory length.

For calculating D_{Res} , instead of removing the jump trajectory segments from the full trajectory, we can also replace these jump trajectory segments by the small step diffusion channel (residual diffusion) during the time taken by the jumps. This can give a stronger proof that D_{Jump} is responsible for the violation of the SE relation. If the jumps last a fraction f of the total time interval t_{traj} , the residual trajectories last a total time $(1 - f)t_{\text{traj}}$, contributing to the MSD for an amount $\text{MSD}_{\text{Res}} = 6D_{\text{Res}}t$. If the jumps are replaced by residual trajectory segments, the new MSD would be $\text{MSD}_{\text{Res}}(\text{Modified}) = 6D_{\text{Res}}(\text{eff})t = 6D_{\text{Res}}/(1 - f)t$, which is equivalent to an effective residual diffusion coefficient $D_{\text{Res}}(\text{eff}) = D_{\text{Res}}/(1 - f)$. f can be calculated from P_{Jump} by the following equation $f = P_{\text{Jump}}/100$. P_{Jump} values for different temperatures are listed in Table 4. We have plotted, in Figure S10 of the Supporting Information, $D_{\text{Res}}(\text{eff})\eta/T$ as a function of time. Clearly, the difference between $D_{\text{Res}}(\text{eff})\eta/T$ and $D_{\text{Res}}\eta/T$ is very small. This is because f is very small at all temperatures, and the effect is maximum ($\sim 5\%$) at 210 K.

4. CONCLUSIONS

In conclusion, we have presented an MD simulation analysis for quantitative estimation of the role of translational jump diffusion on the increasing decoupling of viscosity from the translational diffusion with decreasing temperature. By careful consideration of the translational jump trajectories of the water molecules, we have calculated the jump-only diffusion coefficient D_{Jump} . As the temperature is decreased, the contribution of D_{Jump} to the overall diffusion increases. By subtracting D_{Jump} from D , we obtain the residual diffusion coefficient D_{Res} . While D_{Jump} intensely decouples from the viscosity η , D_{Res} stays coupled fairly strongly with η at all the temperatures studied. This is a clear proof for the growing importance of translational jump diffusion of the molecules for the observed breakdown of the SE equation with decreasing temperature.

These new findings can help in elucidating many experimental studies featuring molecular transport properties in a more complex chemical and biological environment, where

strong diffusion–viscosity decoupling is prevalent. Also, a modified version of the above methodology can be used for calculating the rotational jump-only diffusion coefficient for a nonassociated liquid. This would generalize the existing rotational jump model for liquid water.^{82,83}

Last, we have observed continuous change of various simulated quantities, total diffusion coefficient D , viscosity coefficient η , $D\eta/T$, jump diffusion coefficient D_{jump} , percentage contribution of the jump diffusion to the overall diffusion $100(D_{\text{jump}}/D)\%$, etc., on the decreasing temperature of the medium without an abrupt change as the simulated Widom line is crossed. This is because the pressure is maintained at 1 bar in the present simulation, which is much less than the simulated critical pressure for TIP4P/2005 water ($T = 193$ K, $p = 1350$ bar).⁷⁰ The effect of the Widom line position is generally observed once the simulated condition reaches close to the LLC. Further studies (e.g., pressure dependence on jump diffusion coefficient) are required in this front.

■ ASSOCIATED CONTENT

● Supporting Information

The Supporting Information is available free of charge on the ACS Publications website at DOI: 10.1021/acs.jpcb.9b01719.

Comparison between simulated and experimental density, comparison between simulated and experimental dynamical properties, dependence of the results on input parameters, comparison between simulated and theoretical van Hove correlation functions, some examples of jump and cage trajectories for all the temperatures, section for error analysis, derivation of eq 6 of the main text ($D_{\text{jump}} = \frac{1}{6} \nu_{\text{jump}} \lambda_{\text{jump}}^2$) from random walk problem, and direct evaluation of D_{jump} and D_{Res} values using the MSD route (PDF)

■ AUTHOR INFORMATION

Corresponding Author

*E-mail: snehasis@iitp.ac.in

ORCID

Snehasis Daschakraborty: 0000-0002-2694-7142

Author Contributions

[†]S.D. and V.D. contributed equally.

Notes

The authors declare no competing financial interest.

■ ACKNOWLEDGMENTS

We acknowledge Prof. James T. Hynes, Prof. Jannis Samios, Prof. Claudio E. Margulis, Prof. Ranjit Biswas, and Dr. Sandipa Indra for fruitful discussion and IIT Patna for the computational facility. S.D. and V.D. acknowledge IIT Patna for their research fellowships. We acknowledge the anonymous reviewers for their constructive criticism and continuous effort for enhancing the quality of the work.

■ REFERENCES

- (1) Qvist, J.; Mattea, C.; Sunde, E. P.; Halle, B. Rotational dynamics in supercooled water from nuclear spin relaxation and molecular simulations. *J. Chem. Phys.* **2012**, *136*, 204505.
- (2) Chen, S.-H.; Mallamace, F.; Mou, C.-Y.; Broccio, M.; Corsaro, C.; Faraone, A.; Liu, L. The violation of the Stokes-Einstein relation in supercooled water. *Proc. Natl. Acad. Sci. U.S.A.* **2006**, *103*, 12974–12978.
- (3) Kumar, P. Breakdown of the Stokes-Einstein relation in supercooled water. *Proc. Natl. Acad. Sci. U.S.A.* **2006**, *103*, 12955–12956.
- (4) Dehaoui, A.; Issenmann, B.; Caupin, F. Viscosity of deeply supercooled water and its coupling to molecular diffusion. *Proc. Natl. Acad. Sci. U.S.A.* **2015**, *112*, 12020–12025.
- (5) Cicerone, M. T.; Ediger, M. D. Enhanced translation of probe molecules in supercooled o-terphenyl: Signature of spatially heterogeneous dynamics? *J. Chem. Phys.* **1996**, *104*, 7210–7218.
- (6) Ediger, M. D. Spatially heterogeneous dynamics in supercooled liquids. *Annu. Rev. Phys. Chem.* **2000**, *51*, 99–128.
- (7) Fujara, F.; Geil, B.; Sillescu, H.; Fleischer, G. Translational and rotational diffusion in supercooled orthoterphenyl close to the glass transition. *Z. Phys. B: Condens. Matter* **1992**, *88*, 195–204.
- (8) Chang, I.; Fujara, F.; Geil, B.; Heuberger, G.; Mangel, T.; Sillescu, H. Translational and rotational molecular motion in supercooled liquids studied by NMR and forced Rayleigh scattering. *J. Non-Cryst. Solids* **1994**, *172–174*, 248–255.
- (9) Debenedetti, P. G.; Stillinger, F. H. Supercooled liquids and the glass transition. *Nature* **2001**, *410*, 259.
- (10) Banerjee, P.; Yashonath, S.; Bagchi, B. Rotation driven translational diffusion of polyatomic ions in water: A novel mechanism for breakdown of Stokes-Einstein relation. *J. Chem. Phys.* **2017**, *146*, 164502.
- (11) Guchhait, B.; Daschakraborty, S.; Biswas, R. Medium decoupling of dynamics at temperatures ~ 100 K above glass-transition temperature: A case study with (acetamide + lithium bromide/nitrate) melts. *J. Chem. Phys.* **2012**, *136*, 174503.
- (12) Park, Y.; Kim, J.; Sung, B. J. Translation-rotation decoupling of tracers of locally favorable structures in glass-forming liquids. *J. Chem. Phys.* **2017**, *147*, 124503.
- (13) Acharya, S.; Nandi, M. K.; Mandal, A.; Sarkar, S.; Bhattacharyya, S. M. Diffusion of Small Solute Particles in Viscous Liquids: Cage Diffusion, a Result of Decoupling of Solute-Solvent Dynamics, Leads to Amplification of Solute Diffusion. *J. Phys. Chem. B* **2015**, *119*, 11169–11175.
- (14) Cicerone, M. T.; Ediger, M. D. Enhanced translation of probe molecules in supercooled o-terphenyl: Signature of spatially heterogeneous dynamics? *J. Chem. Phys.* **1996**, *104*, 7210.
- (15) Richert, R. Heterogeneous dynamics in liquids: fluctuations in space and time. *J. Phys.: Condens. Matter* **2002**, *14*, R703–R738.
- (16) Cicerone, M. T.; Ediger, M. D. Relaxation of spatially heterogeneous dynamic domains in supercooled ortho-terphenyl. *J. Chem. Phys.* **1995**, *103*, 5684.
- (17) Kaufman, L. J. Heterogeneity in Single-Molecule Observables in the Study of Supercooled Liquids. *Annu. Rev. Phys. Chem.* **2013**, *64*, 177–200.
- (18) Cicerone, M. T.; Zhong, Q.; Tyagi, M. Picosecond Dynamic Heterogeneity, Hopping, and Johari-Goldstein Relaxation in Glass-Forming Liquids. *Phys. Rev. Lett.* **2014**, *113*, 117801.
- (19) Giovambattista, N.; Mazza, M. G.; Buldyrev, S. V.; Starr, F. W.; Stanley, H. E. Dynamic Heterogeneities in Supercooled Water†. *J. Phys. Chem. B* **2004**, *108*, 6655–6662.
- (20) Kob, W.; Donati, C.; Plimpton, S. J.; Poole, P. H.; Glotzer, S. C. Dynamical Heterogeneities in a Supercooled Lennard-Jones Liquid. *Phys. Rev. Lett.* **1997**, *79*, 2827–2830.
- (21) Karmakar, S.; Dasgupta, C.; Sastry, S. Growing length and time scales in glass-forming liquids. *Proc. Natl. Acad. Sci. U.S.A.* **2009**, *106*, 3675–3679.
- (22) Yamamoto, R.; Onuki, A. Dynamics of highly supercooled liquids: Heterogeneity, rheology, and diffusion. *Phys. Rev. A: At., Mol., Opt. Phys.* **1998**, *58*, 3515–3529.
- (23) Andersen, H. C. Molecular dynamics studies of heterogeneous dynamics and dynamic crossover in supercooled atomic liquids. *Proc. Natl. Acad. Sci. U.S.A.* **2005**, *102*, 6686–6691.
- (24) Dubey, V.; Kumar, N.; Daschakraborty, S. Importance of Solvents' Translational-Rotational Coupling for Translational Jump of

a Small Hydrophobic Solute in Supercooled Water. *J. Phys. Chem. B* **2018**, *122*, 7569–7583.

(25) Kawasaki, T.; Kim, K. Identifying time scales for violation/preservation of Stokes-Einstein relation in supercooled water. *Sci. Adv.* **2017**, *3*, No. e1700399.

(26) Guillaud, E.; Merabia, S.; de Ligny, D.; Joly, L. Decoupling of viscosity and relaxation processes in supercooled water: a molecular dynamics study with the TIP4P/2005f model. *Phys. Chem. Chem. Phys.* **2017**, *19*, 2124–2130.

(27) Galamba, N. On the hydrogen-bond network and the non-Arrhenius transport properties of water. *J. Phys.: Condens. Matter* **2017**, *29*, 015101.

(28) Giovambattista, N.; Mazza, M. G.; Buldyrev, S. V.; Starr, F. W.; Stanley, H. E. Dynamic Heterogeneities in Supercooled Water†. *J. Phys. Chem. B* **2004**, *108*, 6655–6662.

(29) Kumar, P.; Buldyrev, S. V.; Becker, S. R.; Poole, P. H.; Starr, F. W.; Stanley, H. E. Relation between the Widom line and the breakdown of the Stokes-Einstein relation in supercooled water. *Proc. Natl. Acad. Sci. U.S.A.* **2007**, *104*, 9575–9579.

(30) Furukawa, A.; Kim, K.; Saito, S.; Tanaka, H. Anisotropic Cooperative Structural Rearrangements in Sheared Supercooled Liquids. *Phys. Rev. Lett.* **2009**, *102*, 016001.

(31) Parmar, A. D. S.; Sengupta, S.; Satry, S. Length-Scale Dependence of the Stokes-Einstein and Adam-Gibbs Relations in Model Glass Formers. *Phys. Rev. Lett.* **2017**, *119*, 056001.

(32) Kumar, P. Breakdown of the Stokes-Einstein relation in supercooled water. *Proc. Natl. Acad. Sci. U.S.A.* **2006**, *103*, 12955–12956.

(33) Goldstein, M. Viscous liquids and the glass transition: a potential energy barrier picture. *J. Chem. Phys.* **1969**, *51*, 3728–3739.

(34) Sastry, S.; Debenedetti, P. G.; Stillinger, F. H. Signatures of distinct dynamical regimes in the energy landscape of a glass-forming liquid. *Nature* **1998**, *393*, 554–557.

(35) Mukherjee, A.; Bhattacharyya, S.; Bagchi, B. Pressure and temperature dependence of viscosity and diffusion coefficients of a glassy binary mixture. *J. Chem. Phys.* **2002**, *116*, 4577–4586.

(36) Bhattacharyya, S.; Bagchi, B. Anisotropic local stress and particle hopping in a deeply supercooled liquid. *Phys. Rev. Lett.* **2002**, *89*, 025504.

(37) Cicerone, M. T.; Zhong, Q.; Tyagi, M. Picosecond dynamic heterogeneity, hopping, and Johari-Goldstein relaxation in glass-forming liquids. *Phys. Rev. Lett.* **2014**, *113*, 117801.

(38) Pastore, R.; Coniglio, A.; Pica, M. From cage-jump motion to macroscopic diffusion in supercooled liquids. *Soft Matter* **2014**, *10*, 5724–5728.

(39) Pica Ciamarra, M. P.; Pastore, R.; Coniglio, A. Particle jumps in structural glasses. *Soft Matter* **2016**, *12*, 358–366.

(40) Bhattacharyya, S. M.; Bagchi, B.; Wolynes, P. G. Facilitation, complexity growth, mode coupling, and activated dynamics in supercooled liquids. *Proc. Natl. Acad. Sci. U.S.A.* **2008**, *105*, 16077–16082.

(41) Van Der Spoel, D.; Lindahl, E.; Hess, B.; Groenhof, G.; Mark, A. E.; Berendsen, H. J. C. GROMACS: Fast, Flexible, and Free. *J. Comput. Chem.* **2005**, *26*, 1701–1718.

(42) Abascal, J. L. F.; Vega, C. A general purpose model for the condensed phases of water: TIP4P/2005. *J. Chem. Phys.* **2005**, *123*, 234505.

(43) Nosé, S. A Unified Formulation of the Constant Temperature Molecular Dynamics Methods. *J. Chem. Phys.* **1984**, *81*, 511–519.

(44) Hoover, W. G. Canonical Dynamics: Equilibrium Phase-Space Distributions. *Phys. Rev. A* **1985**, *31*, 1695–1697.

(45) Parrinello, M.; Rahman, A. Polymorphic Transitions in Single Crystals: A New Molecular Dynamics Method. *J. Appl. Phys.* **1981**, *52*, 7182–7190.

(46) Hess, B.; Bekker, H.; Berendsen, H. J. C.; Fraaije, J. G. E. M. LINCS: A Linear Constraint Solver for Molecular Simulations. *J. Comput. Chem.* **1997**, *18*, 1463–1472.

(47) Schufle, J. A.; Venugopalan, M. Specific volume of liquid water to -40°C . *J. Geophys. Res.* **1967**, *72*, 3271–3275.

(48) Kell, G. S. Density, thermal expansivity, and compressibility of liquid water from 0.deg. to 150.deg.. Correlations and tables for atmospheric pressure and saturation reviewed and expressed on 1968 temperature scale. *J. Chem. Eng. Data* **1975**, *20*, 97–105.

(49) Hare, D. E.; Sorensen, C. M. The density of supercooled water. II. Bulk samples cooled to the homogeneous nucleation limit. *J. Chem. Phys.* **1987**, *87*, 4840.

(50) González, M. A.; Valeriani, C.; Caupin, F.; Abascal, J. L. F. A comprehensive scenario of the thermodynamic anomalies of water using the TIP4P/2005 model. *J. Chem. Phys.* **2016**, *145*, 054505.

(51) Sumi, T.; Sekino, H. Effects of hydrophobic hydration on polymer chains immersed in supercooled water. *RSC Adv.* **2013**, *3*, 12743–12750.

(52) Price, W. S.; Ide, H.; Arata, Y. Self-Diffusion of Supercooled Water to 238 K Using PGSE NMR Diffusion Measurements. *J. Phys. Chem. A* **1999**, *103*, 448–450.

(53) Montero de Hijes, P.; Sanz, E.; Joly, L.; Valeriani, C.; Caupin, F. Viscosity and self-diffusion of supercooled and stretched water from molecular dynamics simulations. *J. Chem. Phys.* **2018**, *149*, 094503.

(54) Sengupta, S.; Karmakar, S. Distribution of diffusion constants and Stokes-Einstein violation in supercooled liquids. *J. Chem. Phys.* **2014**, *140*, 224505.

(55) Shi, R.; Russo, J.; Tanaka, H. Origin of the emergent fragile-to-strong transition in supercooled water. *Proc. Natl. Acad. Sci. U.S.A.* **2018**, *115*, 9444.

(56) Angell, C. A. Water II is a “strong” liquid. *J. Phys. Chem.* **1993**, *97*, 6339.

(57) Ito, K.; Moynihan, C. T.; Angell, C. A. Thermodynamic determination of fragility in liquids and a fragile-to-strong liquid transition in water. *Nature* **1999**, *398*, 492.

(58) Gainaru, C.; Agapov, A. L.; Fuentes-Landete, V.; Amann-Winkel, K.; Nelson, H.; Köster, K. W.; Kolesnikov, A. I.; Novikov, V. N.; Richert, R.; Böhmer, R.; Loerting, T.; Sokolov, A. P. Anomalous large isotope effect in the glass transition of water. *Proc. Natl. Acad. Sci. U.S.A.* **2014**, *111*, 17402.

(59) Loerting, T.; Fuentes-Landete, V.; Handle, P. H.; Seidl, M.; Amann-Winkel, K.; Gainaru, C.; Böhmer, R. The glass transition in high-density amorphous ice. *J. Non-Cryst. Solids* **2015**, *407*, 423.

(60) Saito, S.; Bagchi, B.; Ohmine, I. Crucial role of fragmented and isolated defects in persistent relaxation of deeply supercooled water. *J. Chem. Phys.* **2018**, *149*, 124504.

(61) Kumar, S. K.; Szamel, G.; Douglas, J. F. Nature of the breakdown in the Stokes-Einstein relationship in a hard sphere fluid. *J. Chem. Phys.* **2006**, *124*, 214501.

(62) Eaves, J. D.; Reichman, D. R. Spatial dimension and the dynamics of supercooled liquids. *Proc. Natl. Acad. Sci. U.S.A.* **2009**, *106*, 15171.

(63) Charbonneau, B.; Charbonneau, P.; Jin, Y.; Parisi, G.; Zamponi, F. Dimensional dependence of the Stokes-Einstein relation and its violation. *J. Chem. Phys.* **2013**, *139*, 164502.

(64) Charbonneau, P.; Jin, Y.; Parisi, G.; Zamponi, F. Hopping and the Stokes-Einstein relation breakdown in simple glass formers. *Proc. Natl. Acad. Sci. U.S.A.* **2014**, *111*, 15025.

(65) Mallamace, F.; Branca, C.; Corsaro, C.; Leone, N.; Spooren, J.; Chen, S.-H.; Stanley, H. E. Transport properties of glass-forming liquids suggest that dynamic crossover temperature is as important as the glass transition temperature. *Proc. Natl. Acad. Sci. U.S.A.* **2010**, *107*, 22457.

(66) Yeh, I.-C.; Hummer, G. System-Size Dependence of Diffusion Coefficients and Viscosities from Molecular Dynamics Simulations with Periodic Boundary Conditions. *J. Phys. Chem. B* **2004**, *108*, 15873.

(67) Tazi, S.; Boğan, A.; Salanne, M.; Marry, V.; Turq, P.; Rotenberg, B. Diffusion coefficient and shear viscosity of rigid water models. *J. Phys.: Condens. Matter* **2012**, *24*, 284117.

(68) Abascal, J. L. F.; Vega, C. Widom line and the liquid-liquid critical point for the TIP4P/2005 water model. *J. Chem. Phys.* **2010**, *133*, 234502.

- (69) Hestand, N. J.; Skinner, J. L. Perspective: Crossing the Widom line in no man's land: Experiments, simulations, and the location of the liquid-liquid critical point in supercooled water. *J. Chem. Phys.* **2018**, *149*, 140901.
- (70) Ni, Y.; Hestand, N. J.; Skinner, J. L. Communication: Diffusion constant in supercooled water as the Widom line is crossed in no man's land. *J. Chem. Phys.* **2018**, *148*, 191102.
- (71) Bhattacharyya, S.; Mukherjee, A.; Bagchi, B. Correlated orientational and translational motions in supercooled liquids. *J. Chem. Phys.* **2002**, *117*, 2741.
- (72) Takeuchi, H. A jump motion of small molecules in glassy polymers: A molecular dynamics simulation. *J. Chem. Phys.* **1990**, *93*, 2062.
- (73) Müller-Plathe, F.; Rogers, S. C.; van Gunsteren, W. F. Computational evidence for anomalous diffusion of small molecules in amorphous polymers. *Chem. Phys. Lett.* **1992**, *199*, 237–243.
- (74) Tocci, E.; Hofmann, D.; Paul, D.; Russo, N.; Drioli, E. A molecular simulation study on gas diffusion in a dense poly(ether-ether-ketone) membrane. *Polymer* **2001**, *42*, 521.
- (75) Indra, S.; Daschakraborty, S. Mechanism of translational jump of a hydrophobic solute in supercooled water: Importance of presolvation. *Chem. Phys. Lett.* **2017**, *685*, 322–327.
- (76) Kumar, A. V.; Bhatia, S. K. Mechanisms Influencing Levitation and the Scaling Laws in Nanopores: Oscillator Model. *J. Phys. Chem. B* **2006**, *110*, 3109–3113.
- (77) Raptis, T. E.; Raptis, V. E.; Samios, J. New effective method for quantitative analysis of diffusion jumps, applied in molecular dynamics simulations of small molecules dispersed in short chain systems. *J. Phys. Chem. B* **2007**, *111*, 13683–13693.
- (78) Raptis, T. E.; Raptis, V. E.; Samios, J. Quantitative study of diffusion jumps in atomistic simulations of model gas-polymer systems. *Mol. Phys.* **2012**, *110*, 1171–1178.
- (79) Araque, J. C.; Yadav, S. K.; Shadeck, M.; Maroncelli, M.; Margulis, C. J. How Is Diffusion of Neutral and Charged Tracers Related to the Structure and Dynamics of a Room-Temperature Ionic Liquid? Large Deviations from Stokes-Einstein Behavior Explained. *J. Phys. Chem. B* **2015**, *119*, 7015–7029.
- (80) Shell, M. S.; Debenedetti, P. G.; Stillinger, F. H. Dynamic heterogeneity and non-Gaussian behaviour in a model supercooled liquid. *J. Phys.: Condens. Matter* **2005**, *17*, S4035–S4046.
- (81) Rahman, A. Correlations in the Motion of Atoms in Liquid Argon. *Phys. Rev.* **1964**, *136*, A405–A411.
- (82) Laage, D.; Hynes, J. T. A molecular jump mechanism of water reorientation. *Science* **2006**, *311*, 832–835.
- (83) Laage, D.; Hynes, J. T. On the molecular mechanism of water reorientation. *J. Phys. Chem. B* **2008**, *112*, 14230–14242.